Theoretical prediction of a high-performance two-dimensional type-II $MoSi_2N_4$/As vdW heterostructure for photovoltaic solar cells

Singh, Deobrat; Khossossi, Nabil; Lizárraga, Raquel; Sonvane, Yogesh

DOI
10.1016/j.renene.2024.121802

Publication date
2024

Document Version
Final published version

Published in
Renewable Energy

Renewable Energy 237 (2024) 121802

Contents lists available at ScienceDirect

Renewable Energy

journal homepage: www.elsevier.com/locate/renene

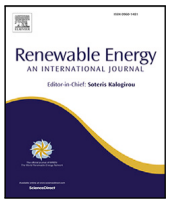

Theoretical prediction of a high-performance two-dimensional type-II $MoSi_2N_4$/As vdW heterostructure for photovoltaic solar cells

Deobrat Singh [a,*], Nabil Khosossi [b], Raquel Lizárraga [a,c], Yogesh Sonvane [d]

[a] Department of Materials Science and Engineering, KTH The Royal Institute of Technology, Stockholm SE-100 44, Sweden
[b] Department of Mechanical Engineering (ME), Delft University of Technology, 2628 CD Delft, The Netherlands
[c] Wallenberg Initiative Materials Science for Sustainability, Department of Materials Science and Engineering, KTH The Royal Institute of Technology, Stockholm SE-100 44, Sweden
[d] Advanced Material Lab, Department of Physics, Sardar Vallabhbhai National Institute of Technology, Surat 395007, India

ARTICLE INFO

Keywords:
2D $MoSi_2N_4$/Arsenene vdW heterostructure
Structural stability
Charge transfer mechanism
Optoelectronic properties
Spectroscopic limited maximum efficiency (SLME)

ABSTRACT

Solar cells are expected to become one of the dominant electricity generation technologies in the coming decades. Developing high-performance absorbers made from thin materials is a promising pathway to improve efficiency and reduce cost, accelerating the widespread adoption of these photovoltaic cells. In the present work, we have systematically investigated the 2D $MoSi_2N_4$/Arsenene van der Waals (vdW) heterostructure, which exhibits a type-II band alignment with an indirect band gap semiconductor (1.58 eV), that can effectively separate the photogenerated electron–hole (e^-–h^+) pairs. Compared to the isolated $MoSi_2N_4$ and Arsenene monolayers, the optical absorption strength can be significantly enhanced in $MoSi_2N_4$/Arsenene vdW heterostructure (in the order of $\sim 10^5$ cm^{-1} in the visible region). The calculated optical absorption gaps are 2.12 eV (Arsenene) and 1.76 eV ($MoSi_2N_4$), with excitonic binding energies of 0.05 eV for arsenene and 0.48 eV for $MoSi_2N_4$, indicating that both materials can effectively form excitons and separate charges. Moreover, we found a high spectroscopic limited maximum efficiency of 27.27% for the $MoSi_2N_4$/Arsenene vdW heterostructure, which is relatively higher compared to previously reported 2D heterostructures. *Ab-initio* molecular dynamics (AIMD) simulations at 300 K, 600 K, and 900 K were conducted to evaluate the thermal stability of the $MoSi_2N_4$/Arsenene heterostructure. Simulations in the presence of water and NO_2 at 300 K were also performed to assess its resilience to humidity and pollutants. The results suggest strong stability under harsh environmental conditions. Our findings demonstrate that the 2D $MoSi_2N_4$/Arsenene vdW heterostructure is an excellent candidate for both photovoltaic device applications and optoelectronic nanodevices.

1. Introduction

The increasing global demand for sustainable, eco-friendly energy is spurring an intensive search for innovative materials that can efficiently and cost-effectively harvest and convert solar energy into usable forms. Among these, photovoltaic materials directly convert solar energy into electricity, while photocatalytic materials are used in processes like artificial photosynthesis to drive reactions such as water splitting, producing high-energy chemical fuels, e.g. hydrogen [1–5]. A suitable and efficient photovoltaic medium must meet certain criteria, namely: (a) high photon capture in the visible and ultraviolet ranges, (b) excellent carrier mobility, (c) acceptable durability and stability under room conditions, and (d) low recombination efficiency of electron (e^-) and hole (h^+) pairs. Additionally, successful photocatalyst materials require precisely adjusted band edges that straddle the water's redox potential. These stringent conditions explain why simple semiconductor photovoltaic and photocatalytic materials are relatively rare. One promising approach to overcoming these challenges involves building heterostructures with type-II band alignments. Type-II heterostructures, formed by stacking different 2D materials, are characterized by the staggered alignment of the conduction band minimum (CBM) and valence band maximum (VBM) of the two materials. They feature rich structures, ultra-thin thickness, and smooth surface interfaces [6]. Most importantly, in type-II heterostructures, photogenerated electrons and holes are spatially separated into different layers, reducing the likelihood of electron–hole (e^-–h^+) recombination [7,8], which is key for obtaining luminous energy [9–11]. From a practical point of view, their thinness makes them particularly appealing for the fabrication of flexible solar cells that can be mounted on various surfaces, such as the roof of a vehicle. Moreover, as certain heterostructures can broaden

* Corresponding author.
E-mail address: deosing@kth.se (D. Singh).

https://doi.org/10.1016/j.renene.2024.121802
Received 2 August 2024; Received in revised form 10 October 2024; Accepted 1 November 2024
Available online 7 November 2024

the spectrum of photo-absorption, enhancing their effectiveness in harnessing the entire solar spectrum, it is important to carefully design these type-II vdW heterostructure materials to effectively boost the performance of solar cell devices.

As a newly synthesized candidate among ternary-elemental two-dimensional (2D) materials, $MoSi_2N_4$ has garnered significant attention in recent years [12–18]. It exhibits semiconductor properties with an indirect experimental band gap of 1.94 eV [12]. First principles calculations have found a band gap of 1.79 eV within the generalized gradient approximation (GGA) method [13,14]. Furthermore, $MoSi_2N_4$ demonstrates high intrinsic e^-/h^+ mobilities of approximately 270/1200 cm^2/Vs, and excellent visible light absorption capacity [14]. Additionally, the 2D $MoSi_2N_4$ monolayer has been predicted to be energetically, dynamically, and thermally stable at high temperatures by theoretical studies [19,20]. Another interesting 2D material with semiconductor properties is, Arsenene, a monolayer of arsenic. Arsenene has an indirect/direct bandgap of 1.63/1.97 eV [21] and excellent electronic characteristics [22]. These remarkable properties make 2D $MoSi_2N_4$ monolayer and Arsenene not only excellent material candidates for efficient photovoltaic and photocatalytic applications but also promising building blocks for 2D vdW heterostructures with the potential to surpass the photovoltaic performance of both pristine monolayers.

Recent studies have explored the electronic and optical properties of the 2D $MoSi_2N_4$/Arsenene [23] and 2D BAs/$MoSi_2N_4$ [24] dW heterostructures using first-principles calculations. These studies revealed that both in-plane and vertical strains can effectively modulate the band alignments and band gaps of these heterostructures. In this study, we focus on the potential of the 2D $MoSi_2N_4$/Arsenene vdW heterostructure as a photovoltaic and photocatalytic material. We examine its geometric structure, thermal stability, electronic properties, charge transfer mechanisms, and optical properties, as well as those of the pristine $MoSi_2N_4$ and Arsenene monolayers, using Density Functional Theory (DFT) calculations [25,26]. Our results show that the work function of the 2D $MoSi_2N_4$/Arsenene vdW heterostructure lies between those of both pristine 2D monolayers, resulting in redistribution of the charge density over the vdW interfacial surface. This redistribution facilitates considerable charge transfer across the interface, generating an internal electric field at the vdW interface. Furthermore, the 2D $MoSi_2N_4$/As vdW heterostructure forms a type-II semiconductor band alignment, which effectively separates the photogenerated e^-–h^+ pairs. We also found that the 2D $MoSi_2N_4$/As vdW heterostructure significantly improves light absorption strength compared to the pristine 2D monolayers.

To further assess the potential of the 2D $MoSi_2N_4$/Arsenene vdW heterostructure for photovoltaic applications, we also investigated its spectroscopic limited maximum efficiency (SLME). The high SLME values obtained for the material, the superior charge transfer at the interface and high optical absorption, strongly suggest that this type-II semiconductor, 2D $MoSi_2N_4$/Arsenene vdW heterostructure is an excellent material candidate for high-performance optoelectronic devices.

In the following section, we describe the computational methods used in this work and in Section 3 we present our results on the pristine $MoSi_2N_4$ and Arsenene monolayers, followed by a comprehensive analysis of the properties of 2D $MoSi_2N_4$/Arsenene vdw heterostructure. Section 4 presents our conclusions.

2. Computational methods

The electronic structure calculations presented in this work are based on the projected augmented wave (PAW) pseudopotential [27] that describes the interactions between core and valence electrons as implemented in the Vienna *Ab initio* Simulation Package (VASP) code [27,28]. The Perdew–Burke–Ernzerhof (PBE) [29] functional is used to describe the exchange–correlation interactions. To account for the vdW interactions between the $MoSi_2N_4$ and Arsenene interface, we employed the Grimme's D3 dispersion correction (PBE-D3) [30]. In order to get accurate electronic bandgaps, we used the hybrid HSE06 functional [31] with a screening parameter (μ) of 0.2 $Å^{-1}$ and mixing parameter (α) of 25%. To prevent the physical interaction between periodic images, we used a 20 Å thick vacuum space along the z-direction.

An energy cutoff of 500 eV was used to describe the valence electrons for the plane-wave basis set. The conjugate-gradient (CG) algorithm was employed during structural optimizations, where ions are fully relaxed until the residual force on each atom is less than 10^{-3} eV/Å. For self-consistent field calculations, the energy convergence criteria is set to 1×10^{-6} eV. K-point meshes with Monkhorst–Pack scheme were sampled as $24 \times 24 \times 1$ for 2D $MoSi_2N_4$ and Arsenene monolayers. Electronic structure calculations for $MoSi_2N_4$/Arsenene vdW heterostructure used a $6 \times 6 \times 1$ k-point mesh.

To investigate charge transfer mechanisms at the $MoSi_2N_4$ and Arsenene interface, we employed the Bader charge approach [32]. Furthermore, we calculated the structural mismatch using the following expression

$$\Delta a = \left(\frac{\left| a_{\text{Arsenene}} - a_{\text{MoSi}_2\text{N}_4} \right|}{a_{\text{MoSi}_2 N_4}} \right) \times 100, \tag{1}$$

and a $(4 \times 4 \times 1)$ supercell for 2D Arsenene monolayer and a $(5 \times 5 \times 1)$ supercell for 2D $MoSi_2N_4$. In Eq. (1), $a_{MoSi_2N_4}$ and $a_{Arsenene}$ represent the lattice parameters of $MoSi_2N_4$ and Arsenene monolayers, respectively. The calculated lattice mismatch Δa was found to be small enough, 0.14% along a and b directions, suggesting that such heterostructure should experience negligible strain which is less than previously investigated work such as MoS_2/Si_2BN (1.4%) [33] and $CH_3NH_3PbI_3/HfS_2$ (3.07%) vdW heterostructure [34]. Minimum lattice mismatch reduces strain within the layers which is essential for the successful fabrication of vdW heterostructures.

In order to check the thermodynamic stability of vdW heterostructure, we investigated the adhesion energy, which can be calculated as

$$E_{\text{adh}} = E_{\text{MoSi}_2\text{N}_4/\text{Arsenene}} - E_{\text{MoSi}_2\text{N}_4} - E_{\text{Arsenene}}, \tag{2}$$

where, $E_{MoSi_2N_4}$, $E_{Arsenene}$ and $E_{MoSi_2N4/Arsenene}$ stand for the total energy of pristine $MoSi_2N_4$, Arsenene and $MoSi_2N_4$/Arsenene vdw heterostructure, respectively. The calculated E_{adh} was found to be −5.77 eV (≈−0.46 meV/$Å^2$) which is relatively lower than that of previously reported vdW heterostructures [33,35].

To gain a deeper understanding of structural stability, the phonon band structure are computed using a finite displacement method within the PHONOPY package [36]. To thoroughly analyze charge transfer, the Bader charge analysis method [32] is employed. Lobster code has been used to investigate the crystal orbital Hamilton population (COHP) for chemical bonding information between the atomic pairs [37].

Additionally, we used VASPKIT software [38] to calculate the valence and conduction band edge positions, carrier effective masses, and transition probability of electrons during post-processing calculations. To understand in depth the electronic properties, the carrier effective mass of pristine $MoSi_2N_4$, Arsenene and vdw heterostructure $MoSi_2N_4$/Arsenene have been calculated. The effective masses of the electrons (m_e^*/m_0) and holes (m_h^*/m_0) at the CBM and VBM of the considered systems are estimated using the following relation:

$$\text{m}^* = (\frac{h}{2\pi})^2 \left[\frac{\partial^2 E(k)}{\partial k^2} \right]^{-1}, \tag{3}$$

where h is the Planck constant, and k is wave vector and E(k) is the energy.

The optical properties of the 2D Arsenene and $MoSi_2N_4$ monolayers were investigated using DFT, the Random Phase Approximation (RPA)

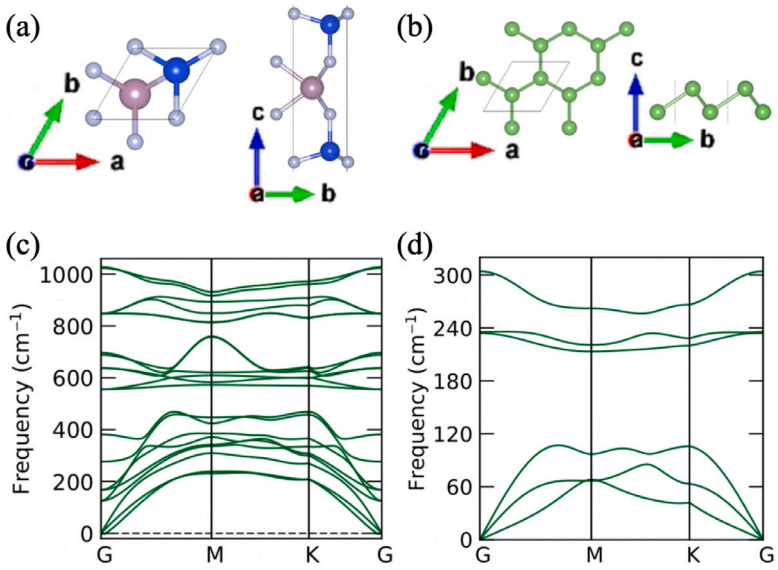

Fig. 1. Fully optimized crystal structures (top and side views) of (a) $MoSi_2N_4$ monolayer, (b) Arsenene monolayer. The phonon dispersion spectra along high symmetry lines of (c) $MoSi_2N_4$ monolayer and (d) Arsenene monolayer.

and the Bethe–Salpeter Equation (BSE) approach in combination with G_0W_0 calculation of a single shot [39] for comparison. It is well known that DFT and RPA approaches do not capture the optical properties properly. Here, to execute the GW approximation effectively, GW calculations are performed with a comprehensive update of both the Green's function (G) and the screened potential (W) [40–42]. The G_0W_0 plus BSE approach takes into account the correlation effects of electron–electron (e–e) and electron–hole (e–h) interactions. The absorption spectra is calculated as follows [43]

$$\alpha = \sqrt{2}\omega\sqrt{[|\,\epsilon(\omega)\,| - \epsilon_1(\omega)]}, \tag{4}$$

where the modulus of the complex dielectric function is

$$|\,\epsilon(\omega)\,| = \sqrt{[\epsilon_1^2(\omega) + \epsilon_2^2(\omega)]}, \tag{5}$$

and ϵ_1 and ϵ_2 are the real and imaginary parts of the dielectric function, respectively [44].

3. Results and discussion

3.1. Structural stability of pristine monolayers

First, we investigate the crystal structures of 2D $MoSi_2N_4$ and Arsenene monolayer. The unit cell of both $MoSi_2N_4$ and Arsenene have hexagonal crystal structure. Fig. 1(a,b) shows the fully optimized crystal structures with top and side views of the $MoSi_2N_4$ and Arsenene monolayers. The optimized lattice parameters a = b = 2.89 Å for $MoSi_2N_4$ and a = b = 3.61 Å for Arsenene monolayer. The bond lengths between atoms Mo–Si, Mo–N, Si–N were found to be 3.41 Å, 2.01 Å and 1.74 Å, respectively in $MoSi_2N_4$ monolayer, whereas the bond length between As–As was 2.51 Å for the Arsenene monolayer. These values are consistent with previously reported values for both monolayers [12,45].

In order to investigate the dynamical stability of both monolayers, the phonon dispersion spectra along high symmetry lines were also calculated. The results are shown in Fig. 1(c,d). No negative frequencies are present in the phonon dispersion spectra of any of the pristine monolayers, demonstrating the dynamical stability of the considered monolayers.

The thermal stability of 2D $MoSi_2N_4$ and Arsenene monolayer was investigated by means of AIMD simulations. Fig. 2(a,b) display the AIMD simulations at 300 K. Energy fluctuations (bottom part of Fig. 2(a,b)) are relatively small with respect to simulation time of up to 5 ps. No breaking of chemical bonds between the atoms in the final structures at 300 K is observed. This implies that the pristine structures of $MoSi_2N_4$ and Arsenene are both thermally stable.

Table 1
Electronic band gap (eV) using PBE and HSE06, effective mass of electron m_e and hole m_h of pristine $MoSi_2N_4$, Arsenene monolayer and $MoSi_2N_4$/Arsenene vdW heterostructure.

Systems	E_g(PBE)	E_g (HSE06)	m_e	m_h
$MoSi_2N_4$	1.77	2.24	0.43	1.18
Arsenene	1.59	2.17	0.52	0.47
$MoSi_2N_4$/Arsenene	1.58	2.54	0.44	1.60

3.2. Electronic and optical properties of pristine 2D $MoSi_2N_4$ and Arsenene monolayer

To understand the electronic properties of the pristine monolayers, we calculated the electronic band structures and the projected density of states (PDOS) for both monolayers. The band structure of $MoSi_2N_4$(Fig. 3a) shows that Mo d-states are the main contributors to the top of the valence band and only a very small part comes from *N* p-states. The same can be observed in the charge density plot of the top of the valence band (see the inset in Fig. 3a) where the charge density surrounds Mo and *N* atoms. Similarly, the bottom of the conduction band consists largely of Mo d-states and a very small part originates from *N* p-states. The charge density can be observed mostly around Mo and *N* atoms at the bottom of the conduction band. The band structure of the Arsenene monolayer (Fig. 3b) shows that the top of the valence band and the bottom of the conduction band are dominated mainly by As p-states. The charge density plot of the top of the valence band and bottom of the conduction band is also presented in the inset of Fig. 3b. The values of the electronic band gap of pristine $MoSi_2N_4$ and Arsenene monolayer are shown in Table 1 and are consistent with previous values in the literature [19,46].

The efficiency of solar cells depends on charge carrier mobility which relates to effective mass. Therefore, we calculated the effective masses of electrons and holes of pristine 2D $MoSi_2N_4$ and Arsenene monolayers. The effective mass of electrons were found to be 0.43 m_0 for $MoSi_2N_4$ and 0.52 m_0 for Arsenene monolayer, whereas the effective mass of holes were 1.18 m_0 and 0.47 m_0 for $MoSi_2N_4$ and

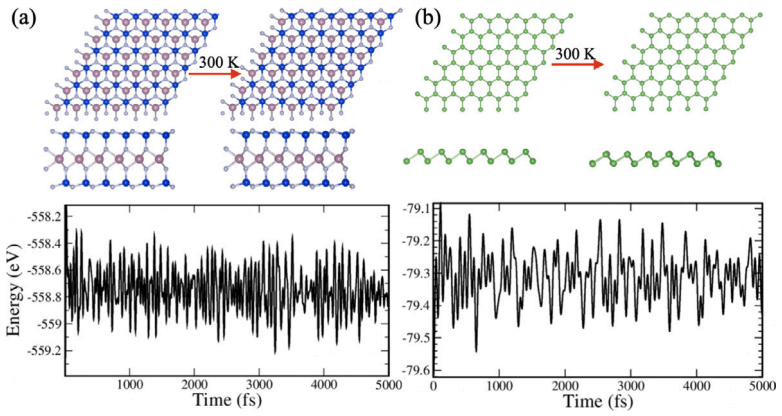

Fig. 2. AIMD simulations at 300 K of (a) $MoSi_2N_4$ and (b) Arsenene monolayer. The top part of the figure displays the initial and final structures at 300 K, whereas the bottom part shows the fluctuations of energy with respect of simulation time.

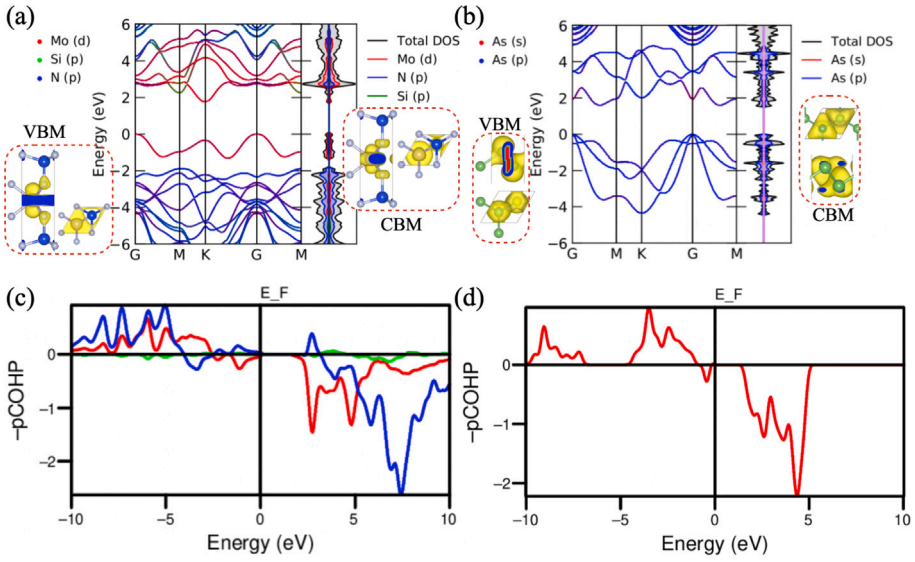

Fig. 3. Elemental- and orbital-resolved electronic band structure along high symmetry lines of pristine (a) $MoSi_2N_4$ and (b) Arsenene monolayer. The inserted part shows the charge density of valence band maximum and conduction band minimum in both pristine monolayers. The red and blue colors appear at the locations of the slicing plane. The COHP analysis of Mo–N (red), Mo–Si (green), Si–N (blue) and As–As (red color) bonding for (c) 2D $MoSi_2N_4$ and (d) Arsenene monolayer. The Fermi level is indicated by a vertical black line set at zero and is located at VBM. Positive and negative values indicate bonding and antibonding nature, respectively.

Arsenene monolayers, respectively (see Table 1). The carrier mobility (μ) is inversely proportional to the effective mass m^*. Since the effective mass of electrons is relatively smaller than that of holes, the carrier mobility of electrons will be larger, which enhances the conductivity.

Next, we performed a COHP analysis to obtain chemical bonding information between the atom-pair following the approach implemented in the Lobster software [37] (see Fig. 3(c,d)). The projected COHP profile provides the chemical bonding strength and shows the bonding, antibonding, and non-bonding contributions to the electronic band structure. Positive and negative values in the profile correspond to bonding and anti-bonding contributions, respectively. We performed the COHP analysis for Mo–N (red), Mo–Si (green), Si–N (blue) atom-pair in 2D $MoSi_2N_4$ monolayer and As–As atom-pair in Arsenene monolayer. We observed that there is no significant anti-bonding contributions in the Mo–N, Mo–Si and Si–N atom-pairs. However, the integrated crystal orbital Hamilton population (-ICOHP) shows negative values; −3.65, −0.14 and −6.75 eV for Mo–N, Mo–Si and Si–N atom-pairs, respectively. This implies strong covalent interactions as can be seen in Fig. 3c. Also, the As–As atom-pair in the case of 2D Arsenene monolayer shows no significant anti-bonding character, and the -ICOHP value is found to be −3.68 eV. This means that there is a strong covalent interaction in As–As atom-pairs as well. Such types of covalent interactions between pairs of atoms provide high stability, and hence greatly enhances catalytic performance.

Furthermore, we calculated the optical properties of pristine 2D $MoSi_2N_4$ and Arsenene monolayer using three approaches; DFT, RPA and BSE for comparison. Benchmarking these approaches against experimental data helps identify the strengths and limitations of each method. Fig. 4(a,b) and (c,d) show the real and imaginary part of the frequency dependent complex dielectric function $\epsilon(\omega)$ for both monolayers, which are calculated by Fermi golden rule and Kramers–Kronig transformation [41]. The real part $\epsilon_1(\omega)$ represents the electronic polarizability of materials, while the imaginary part $\epsilon_2(\omega)$ relates to the interband transition with the light absorption by electrons, which are present in the valence band below the Fermi level (E_F). The calculated static dielectric constants at zero frequency were fount to be 3.27 and 2.54 (DFT), 3.26 and 2.10 (RPA) and 2.93 and 2.35 (BSE) for $MoSi_2N_4$ and Arsenene monolayer, respectively. The real part of dielectric function as calculated by BSE becomes negative for phonon energies between 2.5 to 6 eV for $MoSi_2N_4$ monolayer and 3.1 to 4.3 eV for Arsenene monolayer, which relates to the metallic nature in the visible region as well as in the ultraviolet (UV) region of the electromagnetic (EM) spectrum. In addition, one can observe several peaks in the considered region of EM spectrum of the imaginary

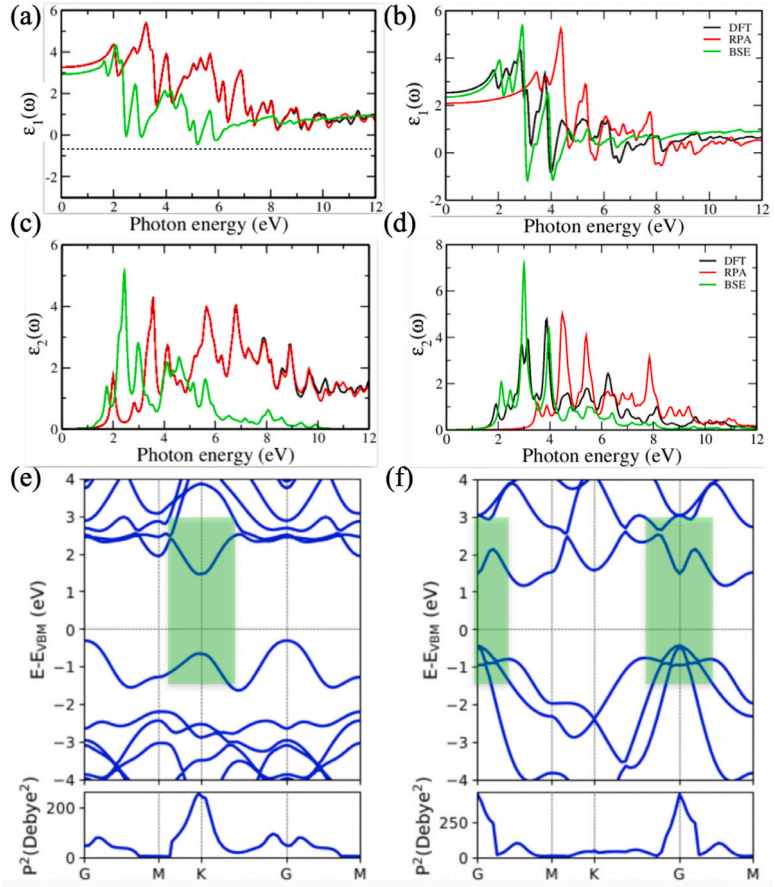

Fig. 4. (a,b) Real and (c,d) imaginary part of the frequency dependent complex dielectric function using DFT, RPA and GW+BSE approaches of pristine $MoSi_2N_4$ and Arsenene monolayer, respectively. (e,f) Transition probability (p^2) corresponding to the electronic band structures of pristine $MoSi_2N_4$ and Arsenene monolayer, respectively. The green shaded region shows the maximum transition probability of electrons from valence to conduction band.

part of dielectric function, which commences at 1.76 eV for $MoSi_2N_4$ monolayer and at 2.12 eV for Arsenene monolayer.

Fig. 4(e,f) display the transition probability of electrons from the valence to the conduction band corresponding to the electronic band structures, and the shaded region indicates the area of maximum transition. The electronic band gaps were found to be 2.24 eV for $MoSi_2N_4$ monolayer and 2.17 eV for Arsenene monolayer using HSE06 approach. Moreover, the excitonic binding energy (EBE) of both pristine 2D $MoSi_2N_4$ and Arsenene monolayer was computed using the following expression

$$\mathrm{EBE} = E_g - E_g^{\mathrm{optical}} \tag{6}$$

where E_g and E_g^{optical} represent the electronic band gap and the first absorption peak from the imaginary part of the dielectric function, respectively. Using Eq. (6), the values for EBE are 0.48 eV and 0.05 eV for $MoSi_2N_4$ and Arsenene monolayers, respectively. These EBE values are lower than that of some of the previously reported 2D monolayered materials [47–50]. Small EBE values can significantly creates holes and electrons and hence effectively enhances the photogenerated electrons and holes.

In Fig. 4(e,f) one can observe that the first absorption peak of the bound excitonic states originates mainly due to the interband transition from valence band to conduction band at high symmetry points K and G (green shaded region in the electronic band structure). This is because the maximum transition probability peaks at K point in $MoSi_2N_4$ monolayer, and at G point in Arsenene monolayer.

Several additional peaks can be seen after that first one in the imaginary part $\epsilon_2(\omega)$ of the 2D $MoSi_2N_4$ monolayer at 1.76 eV, 2.45 eV, 2.99 eV in the visible region and 4.12 eV, 4.58 eV, 5.15 eV, and 5.60 eV in the UV region. These first four peaks of interband transitions occur from pure Mo d-states in the valence band to Mo d-states in the conduction band, whereas the remaining four peaks (in the UV region) originate mainly due to the electronic transition from hybridized orbitals Mo d-states and *N* p-states in the valence band to the d-states of Mo or p-states of *N* (see orbital-resolved electronic band structure in Fig. 3a). Moreover, the first four peaks in the visible region originate mainly at the high symmetry point K, while other transition peaks in the UV region might have arisen at the G point due to the non-zero transition probabilities around G (see Fig. 4e). Similar electronic interband transitions are found by using DFT and RPA approaches but these transitions appeared shifted towards higher photon energy (see Fig. 4(c,d)).

In the case of 2D Arsenene monolayer, we also observed several electronic transitions peaks located at 2.12 eV, 2.48 eV, 3.03 eV in the visible region; and at 3.97 eV, 4.84 eV, 5.48 eV, and 6.40 eV in the UV region as shown in Fig. 4d. The interband transition occurs in the visible region and mainly originates from As p-states in the valence band to the mixed electronic states As s/p-states in the conduction band, which is also confirmed by the maximum transition probability observed at G point in Fig. 4f. The peaks in UV region come mainly from hybridized electronic states s/p-states in the valence band to As s-states or As p-states in the conduction band at G as well as between G-M points. These results demonstrate that the absorption of light covers both the visible and the UV regions in both pristine monolayers.

In summary, we have shown that both monolayers have a good coverage of both visible and UV regions, excellent carrier mobility and can effectively suppress recombination of e^-–h^+ pairs, suggesting that these monolayers are excellent candidates for solar cells and optoelectronic

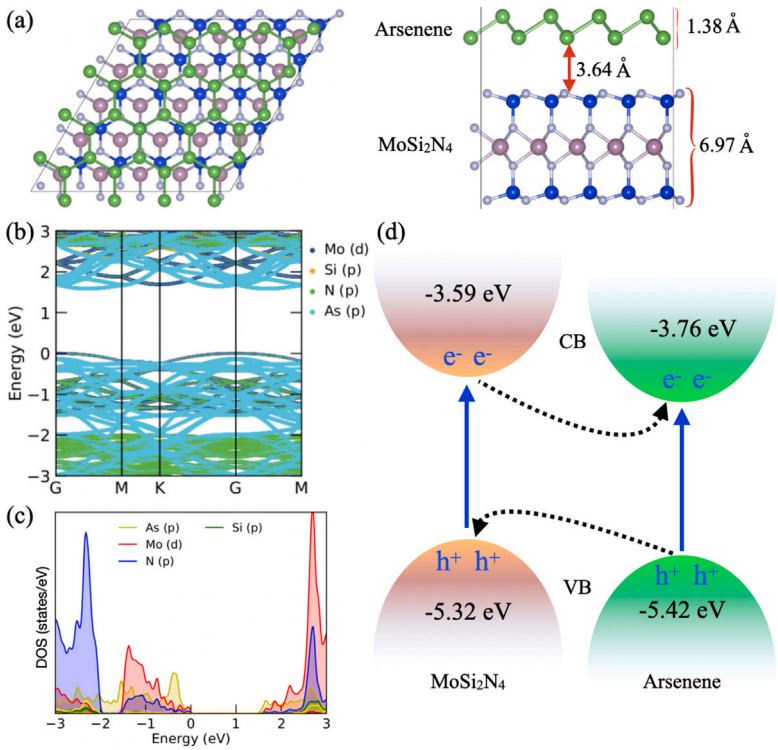

Fig. 5. (a) The vdW heterostructure of $MoSi_2N_4$ and Arsenene monolayer (top and side views). The top surface is Arsenene and the bottom surface is pristine $MoSi_2N_4$. (b) Element- and orbital-resolved electronic band structure, (c) projected density of states of 2D $MoSi_2N_4$/Arsenene vdW heterostructure, and (d) schematic representation of the type-II band alignment and mechanism of charge transfer between $MoSi_2N_4$ and Arsenene monolayer.

devices. In the following we use these two monolayers to construct a $MoSi_2N_4$/Arsenene vdw heterostructure and study its properties.

3.3. Structural stability of $MoSi_2N_4$/Arsenene vdw heterostructure

In previous sections, we studied the stability, the electronic structure, and the optical properties of the building blocks of $MoSi_2N_4$ /Arsenene vdw heterostructure, separately. Now, we proceed to investigate the properties of the heterostructure. Fig. 5a shows the fully optimized structure of 2D $MoSi_2N_4$/Arsenene vdw heterostructure (top and side views). In the present work, we found a very low lattice mismatch of 0.14%, which means that there is a negligible structural strain between them. The optimized vertical distance between $MoSi_2N_4$ and Arsenene monolayer was found to be 3.64 Å and the total thickness of the 2D $MoSi_2N_4$/Arsenene vdW heterostructure was 1.2 nm.

The structural stability of 2D heterostructures is crucial for their practical applications, especially in extreme environments involving high temperatures, humidity, or pollutant gases. Hence, to thoroughly evaluate the robustness of 2D $MoSi_2N_4$/Arsenene vdW heterostructure, we performed AIMD simulations at various temperatures. As illustrated in Fig. S1(a) (see the supplementary material), the potential energy of the heterostructure remained stable across the different simulations at 300 K, 600 K, and 900 K, with only minor fluctuations, confirming the system's stability. At room temperature (300 K), there was no observable atomic displacement or structural degradation after 5 ps, indicating high stability under ambient conditions (shown in Fig. S1(b)). As the temperature increased to 600 K (Fig. S1(c) and 900 K (Fig. S1(d)), the heterostructure maintained its integrity, with no bond dissociation or lattice collapse even under these elevated thermal conditions.

To further assess the stability of the 2D $MoSi_2N_4$/Arsenene heterostructure in humid conditions, we performed AIMD simulations by introducing water molecules at 300 K. As depicted in Fig. S2(a), water molecules were positioned around the heterostructure, and the system's response was monitored over a 5 ps simulation. Despite the potential for hydrogen bonding and chemical interaction with water, the system exhibited stable total energy throughout the simulation, as seen in Fig. S2(b), indicating the absence of significant structural rearrangements or degradation. The mean square displacement (MSD) profile in Fig. S2(c) revealed only limited atomic diffusion, suggesting that no major disruptions occurred at the atomic level. Furthermore, the radial distribution functions (RDFs) for O-As and H-As bonds in Fig. S2(d), as well as for O-N and H-N bonds in Fig. S2(e), showed interactions occurring between the water molecules and the heterostructure. However, no evidence of bond weakening or substantial atomic displacement was observed.

In addition, we investigated the chemical resilience of the 2D $MoSi_2N_4$/Arsenene heterostructure in the presence of atmospheric pollutants, specifically nitrogen dioxide (NO_2), a reactive gas known to degrade materials. To simulate realistic environmental conditions, IMD simulations were performed at 300 K to assess potential chemical reactions between NO_2 molecules and the heterostructure surface. As illustrated in Fig. S3(a), NO_2 molecules were introduced around the heterostructure, and the system's stability was tracked over a 5 ps simulation. Despite the reactive nature of NO_2, the heterostructure demonstrated outstanding stability with no observable structural degradation or bond weakening. The total energy profile, shown in Fig. S3(b), remained stable throughout the simulation, confirming the absence of significant structural rearrangements. MSD in Fig. S3(c) further indicated controlled atomic diffusion without major disruptions.

The results of these simulations combined strongly suggest that the $MoSi_2N_4$/Arsenene vdW heterostructure maintains its structural integrity in the presence of moisture, high temperatures and atmospheric pollutants, underscoring its robustness and suitability for sensitive applications.

3.4. Electronic structure and band alignment of $MoSi_2N_4$/Arsenene vdw heterostructure

We calculated the element- and orbital-resolved electronic band structure and the corresponding projected density of states as shown

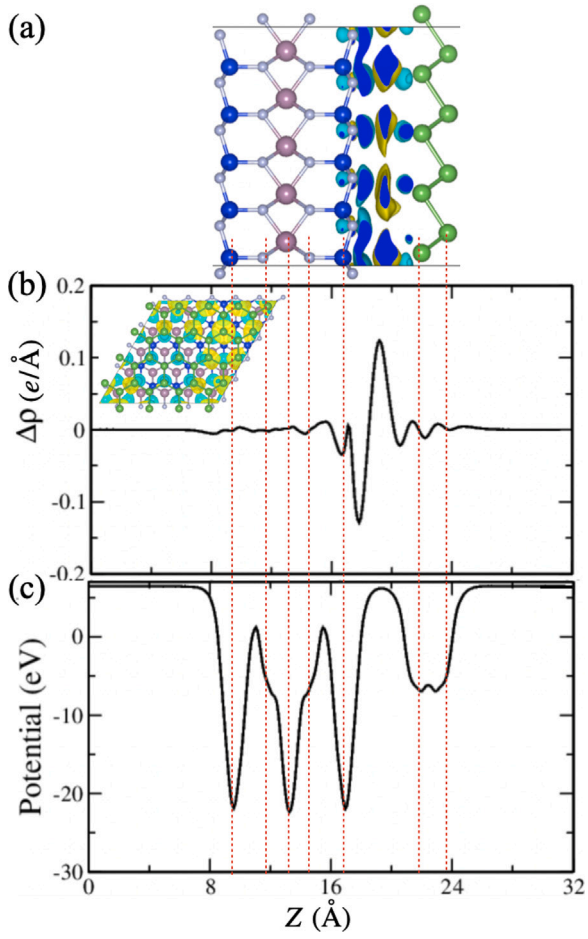

Fig. 6. (a) Side view of charge density difference plot of the 2D $MoSi_2N_4$/Arsenene vdW heterostructure and (b) planar charge density difference plot at the interface of the vdW heterostructure. The insertion shows the top view of charge density difference profile. Charge accumulation region is shown in yellow whereas the charge depletion region is depicted in cyan. (c) Electrostatic potential of the 2D $MoSi_2N_4$/Arsenene vdW heterostructure along the z-direction. The isosurface is set as 1×10^{-4} e/Å^3.

in Fig. 5(b,c). The 2D $MoSi_2N_4$/Arsenene vdW heterostructure exhibits semiconducting behavior with an indirect band gap of 1.58 eV (i.e. G in the valence band and between G-M in the conduction band) (see Table 1). In Fig. 5b, the top of the valence band consists mostly of strongly hybridized orbitals (Mo d-states and N p-states), while the bottom of the conduction band is mainly dominated by pure As p-states. These contributions of electronic states are confirmed by band alignment of 2D $MoSi_2N_4$/Arsenene vdW heterostructure as shown schematically in Fig. 5d. Similar electronic contributions are clearly seen in the projected density of states in Fig. 5c.

Additionally, we investigated the valence band and conduction band edges by means of the VASPKIT package [38] for the considered materials. From the band alignment, it is confirmed that the 2D $MoSi_2N_4$/Arsenene vdW heterostructure exhibits a type-II (staggered) semiconductor characteristic. This indicates that electron transfer originates from the Arsenene monolayer to the $MoSi_2N_4$ monolayer. It is well known that type-II band alignment, which facilitates the transfer of electrons and holes, can effectively suppress recombination at such donor–acceptor hetero-interfaces [34]. From the discussion above, we can conclude that the recombination of charge carriers would be significantly suppressed in this case.

3.5. Charge transfer mechanism in $MoSi_2N_4$/Arsenene vdW heterostructure

In order to study charge transfer mechanisms in the heterostructure, we calculated the charge density difference (CDD) profile for 2D $MoSi_2N_4$/Arsenene vdW heterostructure shown in Fig. 6a. The CDD profile is calculated by using the following expression

$$\Delta\rho = \rho_{(MoSi_2N_4/As)} - \rho_{MoSi_2N_4} - \rho_{Arsenene}, \quad (7)$$

where $\rho_{MoSi_2N_4}$, $\rho_{Arsenene}$ and $\rho_{(MoSi_2N_4/As)}$ are the charge density of $MoSi_2N_4$ monolayer, Arsenene monolayer and $MoSi_2N_4$/Arsenene vdW heterostructure, respectively. Charge accumulation (yellow) and charge depletion (cyan) regions in CDD are depicted in Fig. 6a). In Fig. 6(b), positive values of $\Delta\rho$ indicate charge accumulation, while negative values correspond to charge depletion. It is clear that positive charge appears at the Arsenene monolayer, whereas negative charge originates from the $MoSi_2N_4$ monolayer. This indicates that charge transfer occurs from the Arsenene monolayer to the $MoSi_2N_4$ monolayer. Our Bader charge analysis and work function calculation confirm this result showing that the 2D Arsenene monolayer transfers 0.16 e^- to the $MoSi_2N_4$ surface. Additionally, the direction of charge transfer is confirmed by our calculations of the electrostatic potential (see Fig. 6(c)) and the work functions of the pristine monolayers as well as the vdW heterostructure. The calculated work functions of the pristine 2D $MoSi_2N_4$ and Arsenene monolayers are 5.39 eV and 5.11 eV, respectively, while the 2D $MoSi_2N_4$/Arsenene vdW heterostructure has a work function of 5.30 eV. Thus, the work function of the 2D $MoSi_2N_4$/Arsenene vdW heterostructure lies between those of the pristine 2D $MoSi_2N_4$ and Arsenene monolayers, indicating that charge density is redistributed over the 2D $MoSi_2N_4$/Arsenene vdW interface. Charge transfer always occurs from lower to higher potential, meaning that the Arsenene surface transfers a finite amount of electrons towards the $MoSi_2N_4$ surface. Also, due to the presence of a 0.28 eV electrostatic potential difference, the 2D $MoSi_2N_4$/Arsenene vdW heterostructure generates an internal electric field in which the Arsenene and the $MoSi_2N_4$ surfaces exhibits positive and negative charges, respectively.

There are significant changes in the effective mass of electrons and holes due to the rearrangement of electronic band lines in the band structure of the vdW $MoSi_2N_4$/Arsenene heterostructure. We have calculated the effective masses of electrons and holes to be 0.44 m_0 and 1.60 m_0, respectively (see Table 1). A large difference in the effective masses of the charge carriers can lead to more efficient charge separation and reduced recombination. Such a system significantly enhances the photogenerated e^-–h^+ pairs at the hetero-interface thus enhancing the overall performance of the solar cells.

3.6. Optical properties and SLME of 2D $MoSi_2N_4$/Arsenene vdW heterostructure

Now, we present our results on the optical properties of the 2D $MoSi_2N_4$/Arsenene vdW heterostructure. Fig. 7 shows both the real (a) and imaginary parts (b) of the dielectric function, optical absorption with respect to photon energy, and the transition probability corresponding to the electronic band structure (c). The real part of the dielectric function is presented in Fig. 7(a), where the static dielectric constant at zero frequency is 5.07. This static dielectric constant is significantly larger than those of 2D $MoSi_2N_4$ and Arsenene monolayer, suggesting that the heterostructure built of those monolayers exhibits high electronic polarization. Moreover, $\epsilon_1(\omega)$ is mostly negative above 6.75 eV in the UV region, suggesting that the vdW heterostructure exhibits metallic character when the incident photon energy exceeds 6.75 eV. The first peak of the imaginary part located at 2.01 eV originates primarily from the transitions from Mo d-states in the valence band to As p-states or Mo d-states in the conduction band at the high symmetry point G and between the G-M points. Additionally, several other main peaks are observed at 2.87 eV, 3.62 eV, 4.27 eV, 4.64 eV, 6.27 eV, 6.68 eV, 7.67 eV, and 8.56 eV. The lower excitonic peaks of

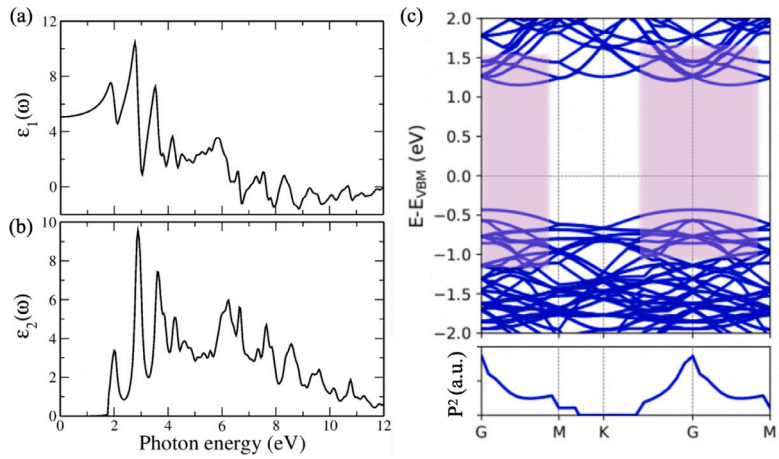

Fig. 7. Frequency dependent optical properties of 2D $MoSi_2N_4$/Arsenene vdW heterostructure, (a) real part (b) imaginary part using GW+BSE approach. (c) Electronic band structure along high symmetry lines and corresponding transition probability p^2 in which the shaded region represents the maximum transition probability of electrons from VB to CB.

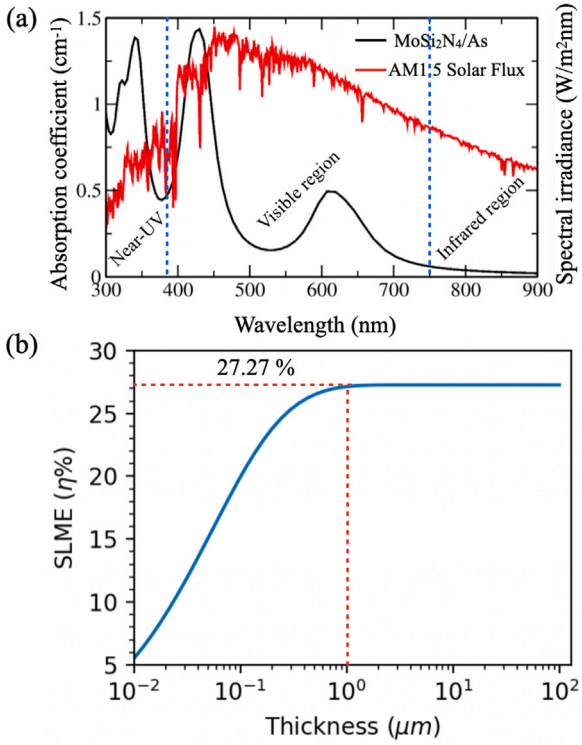

Fig. 8. (a) Calculated optical absorption spectrum (using GW+BSE approach) in the order of 10^6 as a function of photon energy of 2D $MoSi_2N_4$/Arsenene vdW heterostructure superimposed to the incident AM1.5G solar flux, (b) SLME at room temperature as a function of film thickness along the best possible crystal axis of the $MoSi_2N_4$/Arsenene vdW heterostructure.

electronic transitions occur at the high symmetry point G and between G-M points, arising from strongly hybridized orbitals of Mo d-states and *N* p-states in the valence band to As p-states or Mo d-states (see the shaded region in the electronic band structure in Fig. 7c). In contrast, excitonic peaks situated in the higher photon energy region mainly originate from transitions from deep energy levels in the valence band to the conduction band.

To complete our investigation, we also investigated the optical absorption spectra of the 2D $MoSi_2N_4$/Arsenene vdW heterostructure from Eq. (4). We plotted our results in Fig. 8a together with the incident AM1.5G solar flux for comparison. Fig. 8a shows that most of the light absorption covers the solar spectrum including the visible light as well as part of Near-UV (presented in Fig. 8a) for the 2D $MoSi_2N_4$/Arsenene vdW heterostructure. When the visible light and near-UV light are absorbed efficiently, more electrons and holes are generated, leading to better charge separation which contributes to enhance the solar cell efficiency [51,52].

An important parameter for photovoltaic applications is the Spectroscopic Limited Maximum Efficiency (SLME) parameter. The SLME parameter for solar cell devices mainly depends on the optical absorption (data shown in Fig. 8a) and the electronic band gap of the material [34]. Fig. 8b displays our calculated SLME parameter with respect to the thickness of the material. One can observe that the SLME varies significantly from 0.01 μm to 1 μm. In Fig. 8b, the values of SLME increase almost linearly up to 0.7 μm and after that its value saturates, reaching 27.27% at film thickness of 1 μm. The values of SLME in 2D $MoSi_2N_4$/Arsenene vdW heterostructure are significantly larger than those reported for the pristine $MoSi_2N_4$ material (15.44%) [53] and other 2D layered materials [54–59]. Due to the presence of high optical absorption in the order of 10^6 cm^{-1} and the high value of SLME exhibited by 2D $MoSi_2N_4$/Arsenene vdW heterostructure, we conclude that this material is a promising candidate for absorber materials for photovoltaic applications as well as several optoelectronic devices.

4. Conclusions

We investigated for the first time the electronic structure, charge transfer mechanism, and optical properties of 2D $MoSi_2N_4$/Arsenene vdW heterostructure and its 2D components separately using first-principles calculations. The 2D $MoSi_2N_4$/Arsenene vdW heterostructure exhibits high stability and a type-II band alignment with an indirect band gap of 1.58 eV, which can significantly enhance suppression of photogenerated e^-–h^+ pairs. Additionally, we confirmed here that the large difference in the effective mass of electrons and holes effectively separates the e^-–h^+ pairs.

We found that the optical absorption strength of the 2D $MoSi_2N_4$ /Arsenene type-II vdW heterostructure is significantly enhanced due to unique band alignment as compared to the isolated monolayers that compose it. Due to the presence of a 0.28 eV electrostatic potential difference between the 2D $MoSi_2N_4$ and Arsenene monolayers, spontaneous charge transfer from one surface to the other in the $MoSi_2N_4$/Arsenene vdW heterostructure is observed, also generating an internal electric field. The predicted spectroscopic limited maximum efficiency value of the $MoSi_2N_4$/Arsenene vdW heterostructure can reach 27.27%, surpassing that of several other reported vdW

hetero-interfaces. Moreover, the $MoSi_2N_4$/Arsenene vdW heterostructure exhibits excellent thermal stability up to 900 K and strong resilience against moisture and NO_2 exposure, as demonstrated by AIMD simulations. These findings highlight its suitability for practical applications in challenging environments. According to these findings, $MoSi_2N_4$/Arsenene vdW heterostructure meets the demanding criteria for high-performance photovoltaic and photocatalytic materials, making it suitable as absorber in photovoltaic applications. To the best of our knowledge, this heterostructure has not been synthesized. Consequently, we expect that our work will stimulate further experimental research.

CRediT authorship contribution statement

Deobrat Singh: Writing – original draft, Visualization, Methodology, Investigation, Formal analysis. **Nabil Khossossi:** Writing – review & editing, Validation, Methodology, Investigation, Formal analysis, Conceptualization. **Raquel Lizárraga:** Writing – review & editing, Validation, Supervision, Software, Resources, Project administration, Funding acquisition. **Yogesh Sonvane:** Writing – review & editing, Validation, Software, Resources, Funding acquisition.

Declaration of competing interest

The authors declare that they have no known competing financial interests or personal relationships that could have appeared to influence the work reported in this paper.

Acknowledgments

D.S. and R.L. thanks the Carl Tryggers Stiftelse for Vetenskaplig Forskning (CTS 22:2283), Sweden. R.L. would like also to thank the Åforsk Foundation (grant number 22-206). The computations were enabled by resources provided by the National Academic Infrastructure for Supercomputing in Sweden (NAISS), partially funded by the Swedish Research Council, Sweden through grant agreement no. 2022-06725. N.K. acknowledges the computational resources provided by the Dutch Research Organization NWO (Snellius@Surfsara) and DelftBlue supercomputer provided by Delft High-Performance Computing Centre (https://www.tudelft.nl/dhpc). Y.S. is thankful to the Anusandhan National Research Foundation (ANRF), India, for the financial support (grant number: EEQ/2022/000584).

Appendix A. Supplementary data

Supplementary material related to this article can be found online at https://doi.org/10.1016/j.renene.2024.121802.

Data availability statement

The raw/processed data required to reproduce these findings cannot be shared at this time due to legal or ethical reasons. Data are, however, available from the authors upon reasonable request.

References

[1] Y. Qu, X. Duan, Progress, challenge and perspective of heterogeneous photocatalysts, Chem. Soc. Rev. 42 (7) (2013) 2568–2580.
[2] C. Gao, J. Wang, H. Xu, Y. Xiong, Coordination chemistry in the design of heterogeneous photocatalysts, Chem. Soc. Rev. 46 (10) (2017) 2799–2823.
[3] J. Low, J. Yu, M. Jaroniec, S. Wageh, A.A. Al-Ghamdi, Heterojunction photocatalysts, Adv. Mater. 29 (20) (2017) 1601694.
[4] T.V. Vu, N.N. Hieu, D.D. Vo, A. Kartamyshev, H.D. Tong, T.T. Trinh, V. Khuong Dien, Z. Haman, P. Dey, N. Khossossi, 2D Ge2Se2P4 monolayer: A versatile photocatalyst for sustainable water splitting, J. Phys. Chem. C (2024).
[5] Z. Wang, C. Li, K. Domen, Recent developments in heterogeneous photocatalysts for solar-driven overall water splitting, Chem. Soc. Rev. 48 (7) (2019) 2109–2125.
[6] H. Zhao, L. Han, B. Jia, Y. Chen, X. Guan, L. Wu, P. Lu, Type-II van der Waals heterostructures based on AsP and transition metal dichalcogenides: Great promise for applications in solar cell, Phys. Status Solidi (RRL) 16 (2022) 2200043.
[7] Z. Wu, J. Neaton, J.C. Grossman, Charge separation via strain in silicon nanowires, Nano Lett. 9 (6) (2009) 2418–2422.
[8] E.C. Garnett, M.L. Brongersma, Y. Cui, M.D. McGehee, Nanowire solar cells, Annu. Rev. Mater. Sci. 41 (2011) 269–295.
[9] Y. Liu, N.O. Weiss, X. Duan, H.-C. Cheng, Y. Huang, X. Duan, Van der Waals heterostructures and devices, Nat. Rev. Mater. 1 (9) (2016) 1–17.
[10] A.K. Geim, I.V. Grigorieva, Van der Waals heterostructures, Nature 499 (7459) (2013) 419–425.
[11] K. Novoselov, o.A. Mishchenko, o.A. Carvalho, A. Castro Neto, 2D materials and van der Waals heterostructures, Science 353 (6298) (2016) aac9439.
[12] Y.-L. Hong, Z. Liu, L. Wang, T. Zhou, W. Ma, C. Xu, S. Feng, L. Chen, M.-L. Chen, D.-M. Sun, et al., Chemical vapor deposition of layered two-dimensional MoSi2N4 materials, Science 369 (6504) (2020) 670–674.
[13] A. Bafekry, M. Faraji, M. Fadlallah, A.A. Ziabari, A.B. Khatibani, S. Feghhi, M. Ghergherehchi, D. Gogova, Adsorption of habitat and industry-relevant molecules on the MoSi2N4 monolayer, Appl. Surf. Sci. 564 (2021) 150326.
[14] C. Xiao, R. Sa, Z. Cui, S. Gao, W. Du, X. Sun, X. Zhang, Q. Li, Z. Ma, Enhancing the hydrogen evolution reaction by non-precious transition metal (non-metal) atom doping in defective MoSi2N4 monolayer, Appl. Surf. Sci. 563 (2021) 150388.
[15] J. Yu, J. Zhou, X. Wan, Q. Li, High intrinsic lattice thermal conductivity in monolayer MoSi2N4, New J. Phys. 23 (3) (2021) 033005.
[16] Y.-T. Bian, G.-H. Liu, S.-H. Qian, X.-X. Ding, H.-X. Liu, Effect of O-doping or N-vacancy on the structural, electronic and magnetic properties of MoSi2N4 monolayer, 2020, arXiv preprint arXiv:2012.04162.
[17] Z. Sun, J. Xu, N. Mwankemwa, W. Yang, X. Wu, Z. Yi, S. Chen, W. Zhang, Alkali-metal (Li, Na, and K)-adsorbed MoSi2N4 monolayer: an investigation of its outstanding electronic, optical, and photocatalytic properties, Commun. Theor. Phys. (Beijing) 74 (1) (2022) 015503.
[18] W. Qian, Z. Chen, J. Zhang, L. Yin, Monolayer MoSi2N4-x as promising electrocatalyst for hydrogen evolution reaction: A DFT prediction, J. Mater. Sci. Technol. 99 (2022) 215–222.
[19] A. Bafekry, M. Faraji, D.M. Hoat, M. Shahrokhi, M. Fadlallah, F. Shojaei, S. Feghhi, M. Ghergherehchi, D. Gogova, Mosi2n4 single-layer: a novel two-dimensional material with outstanding mechanical, thermal, electronic and optical properties, J. Phys. D: Appl. Phys. 54 (15) (2021) 155303.
[20] C.Q. Nguyen, T.T.P. Le, C.V. Nguyen, First-principles study on the structural and electronic properties of single-layer MoSi2N4, Hue Univ. J. Sci.: Nat. Sci. 131 (1D) (2022) 5–11.
[21] G. Rahman, A. Mahmood, V. García-Suárez, Dynamically stable topological phase of arsenene, Sci. Rep. 9 (2019) 7966.
[22] J. Shah, W. Wang, H.M. Sohail, R. Uhrberg, Experimental evidence of monolayer arsenene: an exotic 2D semiconducting material, 2D Mater. 7 (2) (2020) 025013.
[23] J. Zhao, Y. Qi, C. Yao, H. Zeng, Modulating the electronic properties and band alignments of the arsenene/$MoSi_2N_4$ van der Waals heterostructure via applying strain and electric field, Phys. Chem. Chem. Phys. 25 (48) (2023) 33023–33030.
[24] Y. Qi, C. Yao, J. Zhao, H. Zeng, First principles study of BAs/$MoSi_2N_4$ van der Waals heterostructure: tunable electronic and optical properties via vertical strain, Phys. Chem. Chem. Phys. 25 (41) (2023) 28104–28112.
[25] P. Hohenberg, W. Kohn, Phys. Rev. B 136 (1964) 864.
[26] W. Kohn, L. Sham, Phys. Rev. A 140 (1965) 1133.
[27] B. Hammer, L.B. Hansen, J.K. Nørskov, Improved adsorption energetics within density-functional theory using revised Perdew-Burke-Ernzerhof functionals, Phys. Rev. B 59 (11) (1999) 7413.
[28] G. Kresse, J. Furthmülle, Efficient iterative schemes for ab initio total-energy calculations using a plane-wave basis set, Phys. Rev. B 54 (1996) 11169.
[29] J.P. Perdew, K. Burke, M. Ernzerhof, Generalized gradient approximation made simple, Phys. Rev. Lett. 77 (18) (1996) 3865.
[30] S. Grimme, J. Antony, S. Ehrlich, H. Krieg, A consistent and accurate ab initio parametrization of density functional dispersion correction (DFT-D) for the 94 elements H-Pu, J. Chem. Phys. 132 (15) (2010) 154104.
[31] J. Paier, M. Marsman, K. Hummer, G. Kresse, I.C. Gerber, J.G. Ángyán, Screened hybrid density functionals applied to solids, J. Chem. Phys. 124 (15) (2006) 154709.
[32] E. Sanville, S.D. Kenny, R. Smith, G. Henkelman, Improved grid-based algorithm for Bader charge allocation, J. Comput. Chem. 28 (5) (2007) 899–908.
[33] D. Singh, P.K. Panda, N. Khossossi, Y.K. Mishra, A. Ainane, R. Ahuja, Impact of edge structures on interfacial interactions and efficient visible-light photocatalytic activity of metal–semiconductor hybrid 2D materials, Catal. Sci. Technol. 10 (10) (2020) 3279–3289.
[34] D. Singh, R. Ahuja, Two-dimensional perovskite/HfS2 van der Waals heterostructure as an absorber material for photovoltaic applications, ACS Appl. Energy Mater. (2022).
[35] M. Guo, Y. Yang, Y. Leng, L. Wang, H. Dong, H. Liu, W. Li, Edge dominated electronic properties of MoS 2/graphene hybrid 2D materials: edge state, electron coupling and work function, J. Mater. Chem. C 5 (20) (2017) 4845–4851.

[36] A. Togo, F. Oba, I. Tanaka, First-principles calculations of the ferroelastic transition between rutile-type and CaCl 2-type SiO 2 at high pressures, Phys. Rev. B—Condens. Matter Mater. Phys. 78 (13) (2008) 134106.
[37] S. Maintz, V.L. Deringer, A.L. Tchougréeff, R. Dronskowski, LOBSTER: A tool to extract chemical bonding from plane-wave based DFT, 2016.
[38] V. Wang, N. Xu, J.-C. Liu, G. Tang, W.-T. Geng, VASPKIT: A user-friendly interface facilitating high-throughput computing and analysis using VASP code, Comput. Phys. Comm. 267 (2021) 108033.
[39] M. Shishkin, G. Kresse, Implementation and performance of the frequency-dependent G W method within the PAW framework, Phys. Rev. B 74 (3) (2006) 035101.
[40] D.Y. Qiu, F.H. da Jornada, S.G. Louie, Environmental screening effects in 2D materials: renormalization of the bandgap, electronic structure, and optical spectra of few-layer black phosphorus, Nano Lett. 17 (8) (2017) 4706–4712.
[41] X. Yang, D. Singh, Z. Xu, Z. Wang, R. Ahuja, An emerging Janus MoSeTe material for potential applications in optoelectronic devices, J. Mater. Chem. C 7 (39) (2019) 12312–12320.
[42] A.H. Søndersted, M. Kuisma, J.K. Svaneborg, M.K. Svendsen, K.S. Thygesen, Improved dielectric response of solids: Combining the Bethe-Salpeter equation with the random phase approximation, Phys. Rev. Lett. 133 (2) (2024) 026403.
[43] D. Singh, S.K. Gupta, Y. Sonvane, I. Lukačević, Antimonene: a monolayer material for ultraviolet optical nanodevices, J. Mater. Chem. C 4 (26) (2016) 6386–6390.
[44] F. Wooten, Optical Properties of Solids, Academic Press, 2013.
[45] D. Singh, S.K. Gupta, Y. Sonvane, S. Sahoo, Modulating the electronic and optical properties of monolayer arsenene phases by organic molecular doping, Nanotechnology 28 (49) (2017) 495202.
[46] C. Kamal, M. Ezawa, Arsenene: Two-dimensional buckled and puckered honeycomb arsenic systems, Phys. Rev. B 91 (8) (2015) 085423.
[47] D. Singh, V. Shukla, R. Ahuja, Optical excitations and thermoelectric properties of two-dimensional holey graphene, Phys. Rev. B 102 (7) (2020) 075444.
[48] D.Y. Qiu, H. Felipe, S.G. Louie, Optical spectrum of MoS 2: many-body effects and diversity of exciton states, Phys. Rev. Lett. 111 (21) (2013) 216805.
[49] S. Huang, Y. Liang, L. Yang, Exciton spectra in two-dimensional graphene derivatives, Phys. Rev. B 88 (7) (2013) 075441.
[50] V. Tran, R. Fei, L. Yang, Quasiparticle energies, excitons, and optical spectra of few-layer black phosphorus, 2D Mater. 2 (4) (2015) 044014.
[51] Y. Xu, D. Li, Q. Zeng, H. Sun, P. Li, Type-II 2D AgBr/SiH van der Waals heterostructures with tunable band edge positions and enhanced optical absorption coefficients for photocatalytic water splitting, RSC Adv. 13 (40) (2023) 27676–27685.
[52] C.C. Tho, C. Yu, Q. Tang, Q. Wang, T. Su, Z. Feng, Q. Wu, C. Nguyen, W.-L. Ong, S.-J. Liang, et al., Cataloguing MoSi2N4 and WSi2N4 van der Waals heterostructures: an exceptional material platform for excitonic solar cell applications, Adv. Mater. Interfaces 10 (2) (2023) 2201856.
[53] A. Yadav, J. Kangsabanik, N. Singh, A. Alam, Novel two-dimensional MA2N4 materials for photovoltaic and spintronic applications, J. Phys. Chem. Lett. 12 (2021) 10120–10127.
[54] Y. Chen, Z. Lao, B. Sun, X. Feng, S.A. Redfern, H. Liu, J. Lv, H. Wang, Z. Chen, Identifying the ground-state NP sheet through a global structure search in two-dimensional space and its promising high-efficiency photovoltaic properties, ACS Mater. Lett. 1 (3) (2019) 375–382.
[55] Z. Wang, A.M. Ganose, C. Niu, D.O. Scanlon, First-principles insights into tin-based two-dimensional hybrid halide perovskites for photovoltaics, J. Mater. Chem. A 6 (14) (2018) 5652–5660.
[56] Z. Wang, A.M. Ganose, C. Niu, D.O. Scanlon, Two-dimensional eclipsed arrangement hybrid perovskites for tunable energy level alignments and photovoltaics, J. Mater. Chem. C 7 (17) (2019) 5139–5147.
[57] Y. Guo, J. Min, X. Cai, L. Zhang, C. Liu, Y. Jia, Two-dimensional type-II BP/MoSi2P4 vdW heterostructures for high-performance solar cells, J. Phys. Chem. C (2022).
[58] M.K. Mohanta, A. Rawat, N. Jena, Dimple, R. Ahammed, A. De Sarkar, Interfacing boron monophosphide with molybdenum disulfide for an ultra-high performance in thermoelectrics, two-dimensional excitonic solar cells, and nanopiezotronics, ACS Appl. Mater. Interfaces 12 (2) (2019) 3114–3126.
[59] H. Yang, Y. Ma, Y. Liang, B. Huang, Y. Dai, Monolayer HfTeSe4: a promising two-dimensional photovoltaic material for solar cells with high efficiency, ACS Appl. Mater. Interfaces 11 (41) (2019) 37901–37907.